


# Structural behavior and metallization of $AsSbS_3$ at high pressure

Tian Qin(覃天), Min Wu(武敏), Kai Wang(王凯), Ye Wu(吴也), and Haijun Huang(黄海军)

**Citation:**Chin. Phys. B, 2024, 33 (**11**): 118101. DOI: 10.1088/1674-1056/ad78d8
Journal homepage: http://cpb.iphy.ac.cn; http://iopscience.iop.org/cpb

**What follows is a list of articles you may be interested in**

---

## Recension of boron nitride phase diagram based on high-pressure and high-temperature experiments

Ruike Zhang(张瑞柯), Ruiang Guo(郭睿昂), Qian Li(李倩), Shuaiqi Li(李帅琦), Haidong Long(龙海东), and Duanwei He(贺端威)

Chin. Phys. B, 2024, 33 (**10**): 108103. DOI: 10.1088/1674-1056/ad6a06

## Pressure generation under deformation in a large-volume press

Saisai Wang(王赛赛), Xinyu Zhao(赵鑫宇), Kuo Hu(胡阔), Bingtao Feng(丰丙涛), Xuyuan Hou(侯旭远), Yiming Zhang(张羿鸣), Shucheng Liu(刘书成), Yuchen Shang(尚宇琛), Zhaodong Liu(刘兆东), Mingguang Yao(姚明光), and Bingbing Liu(刘冰冰)

Chin. Phys. B, 2024, 33 (**9**): 098104. DOI: 10.1088/1674-1056/ad58c6

## Diamond growth in a high temperature and high pressure Fe-Ni-C-Si system: Effect of synthesis pressure

Yang Liu(刘杨), Zhiwen Wang(王志文), Bowei Li(李博维), Hongyu Zhao(赵洪宇), Shengxue Wang(王胜学), Liangchao Chen(陈良超), Hongan Ma(马红安), and Xiaopeng Jia(贾晓鹏)

Chin. Phys. B, 2023, 32 (**12**): 128102. DOI: 10.1088/1674-1056/acf03d

## High-pressure and high-temperature sintering of pure cubic silicon carbide: A study on stress-strain and densification

Jin-Xin Liu(刘金鑫), Fang Peng(彭放), Guo-Long Ma(马国龙), Wen-Jia Liang(梁文嘉), Rui-Qi He(何瑞琦), Shi-Xue Guan(管诗雪), Yue Tang(唐越), and Xiao-Jun Xiang(向晓君)

Chin. Phys. B, 2023, 32 (**9**): 098101. DOI: 10.1088/1674-1056/aca6d4

## Synergistic influences of titanium, boron, and oxygen on large-size single-crystal diamond growth at high pressure and high temperature

Guang-Tong Zhou(周广通), Yu-Hu Mu(穆玉虎), Yuan-Wen Song(宋元文), Zhuang-Fei Zhang(张壮飞), Yue-Wen Zhang(张跃文), Wei-Xia Shen(沈维霞), Qian-Qian Wang(王倩倩), Biao Wan(万彪), Chao Fang(房超), Liang-Chao Chen(陈良超), Ya-Dong Li(李亚东), and Xiao-Peng Jia(贾晓鹏)

Chin. Phys. B, 2022, 31 (**6**): 068103. DOI: 10.1088/1674-1056/ac4650

---

# Structural behavior and metallization of $AsSbS_3$ at high pressure

Tian Qin(覃天)[1], Min Wu(武敏)[2], Kai Wang(王凯)[2], Ye Wu(吴也)[1,†], and Haijun Huang(黄海军)[1]

[1] *School of Science, Wuhan University of Technology, Wuhan* 430070, *China*

[2] *Shandong Key Laboratory of Optical Communication Science and Technology, School of Physics Science and Information Technology, Liaocheng University, Liaocheng* 252000, *China*

(Received 8 July 2024; revised manuscript received 6 September 2024; accepted manuscript online 10 September 2024)

The group V–VI semiconductor material getchellite (crystalline $AsSbS_3$) has garnered extensive attention due to its wonderful electronic and optical properties. The pressure engineering is one of the most effective methods to modulate crystal structure and physical properties of semiconductor materials. In this study, the structural behavior, optical and electrical properties of $AsSbS_3$ under high pressure have been investigated systematically by *in situ* high-pressure experiments for the first time. The monoclinic structure of $AsSbS_3$ remains stable up to 47.0 GPa without phase transition. The gradual lattice contraction with increasing pressure results in a continuous narrowing of the bandgap then leads to pressure-induced metallization of $AsSbS_3$ at 31.5 GPa. Our research presents a high-pressure strategy for tuning the crystal structure and physical properties of $AsSbS_3$ to expand its potential applications in electronic and optoelectronic fields.

**Keywords:** $AsSbS_3$, structural behavior, pressure-induced metallization, high pressure

**PACS:** 81.40.Vw, 61.50.Ks, 71.20.Mq, 72.80.Cw **DOI:** 10.1088/1674-1056/ad78d8

## 1. Introduction

The family of group V–VI compounds form a large group of materials that hold significant role in both practical applications and basic science, garnering extensive attention in recent years.[1–4] These materials possess excellent thermoelectric, electronic and optical properties, leading to their widespread use in these domains.[5–8] A significant portion of the V–VI compounds crystallize in a quasi-two-dimensional layered structure, rendering them susceptible to external disturbances. Pressure engineering can significantly alter the properties of matter by substantially changing atomic distances, bonding, and stacking symmetry. Therefore, high pressure has been widely applied in optimizing the thermoelectric, electronic transport, optical, and even superconducting research of high-performance materials.[9–12] Recently, we have conducted a series of studies on IV–VI group layered semiconductor materials and provide a strategy for modulating at high pressure. For instance, the pressure-induced two phase transitions of SnSe from *Pnma* to *Cmcm* and $Pm\bar{3}m$; the pressure-induced bandgap engineering and metallization of 4H-$SnS_2$.[13–15] Hence, carrying out the investigation of various phase transitions and physical properties of V–VI group compounds with similar approach would facilitate the discovery of functional materials and the development of functional devices.

As an emerging V–VI group natural mineral, getchellite ($AsSbS_3$) exhibits the characteristics of a direct bandgap semiconductor, featuring a quasi-two-dimensional layered structure and crystallizes in a monoclinic structure (space group $P2_1/a$).[16] In the unit cell of $AsSbS_3$, each As or Sb atom forms a strong coordination with three S atoms, resulting in the formation of a pyramidal unit. However, the different atomic radii of Sb and As result in different crystal structures between $AsSbS_3$ and other V–VI group compounds, such as stibnite ($Sb_2S_3$) and orpiment ($As_2S_3$).[1,2] These pyramids in $AsSbS_3$ are interconnected through the bonding of each S atom to two neighboring As or Sb atoms, forming an eight-membered ring $As(Sb)_8S_8$ parallel to the (010) plane. Overall, the $AsSbS_3$ layers parallel to the [001] direction are combined by weak van der Waals (vdW) forces, creating its quasi-two-dimensional layered structure (the inset in Fig. 1(b)). Furthermore, the distribution of cations among the 40 atoms in the $AsSbS_3$ unit cell (16 As/Sb atoms and 24 S atoms) exhibits disorder, with four different distribution preferences at four distinct sites, M1–M4, which is believed to be caused by the slow crystallization process occurring in nature.[17,18] Moreover, $AsSbS_3$ is characterized by a direct bandgap of 1.74 eV. It is also deemed to exhibit electrical properties comparable to those of superior semiconductors such as $MoS_2$, in addition to various anisotropic optical properties.[19–21] Such characteristics suggest its potential applicability in high-performance optoelectronic devices, including photodetectors, optical sensors, and nonlinear optical signal processors.

Although $AsSbS_3$ has wonderful potential for applications and optimization, and its structure is compatible with enhancements through pressure engineering, research on $AsSbS_3$ under high pressure is still an unexplored area. In this work, the structural behavior, optical, and electrical properties of $AsSbS_3$ under high pressure were systematically investigated by experiments for the first time. The *in situ* high pres-

†Corresponding author. E-mail: yew@whut.edu.cn

© 2024 Chinese Physical Society and IOP Publishing Ltd 

sure x-ray diffraction (HP-XRD) and Raman spectroscopy experiments up to 50 GPa were conducted, which facilitated the acquisition of compelling evidence needed to understand the structural behavior of $AsSbS_3$ within the studied range. Additionally, absorption spectra measurements were conducted up to 24.5 GPa, furnishing critical insights into the modulation of the bandgap in $AsSbS_3$ subjected under high pressure.[22] The electrical transport properties of $AsSbS_3$ were also measured using the van der Pauw four-probe method, indicating the pathway to pressure-induced metallization of $AsSbS_3$.[23]

## 2. Sample and experimental details

### 2.1. Sample characterizations

In this work, natural crystalline $AsSbS_3$ was gathered from Nevada, USA. The XRD and electron microprobe analysis were utilized to determine the crystal structure and chemical composition of the natural sample. The natural sample crystallizes in a monoclinic structure ($P2_1/a$, $Z = 8$) with lattice parameters $a = 11.81$ Å, $b = 9.02$ Å, $c = 10.17$ Å, $\beta = 116.61°$, and $V = 968.13$ Å$^3$ (Fig. S1 in supporting information). The getchellite has a chemical composition of $As_{0.949}Sb_{1.047}S_{3.004}$ (Table S1).

### 2.2. Experimental details

A symmetric-type or BX90 diamond anvil cell (DAC), featuring a diameter anvil culet of 300 μm, was used to produce high pressure.[24] Gaskets made of T-301 stainless steel were pre-indented to a thickness ranging between 30 μm to 40 μm. Subsequently, cavities of 120 μm in diameter were drilled in the pre-indented gaskets as the sample chamber. Either argon gas, NaCl or silicone oil was used as the pressure transmitting medium (PTM), and pressure calibration was performed using fluorescence of ruby or high-frequency Raman shift of diamond.[25,26] The HP-XRD measurements were performed at the BL15U1 beamline of the Shanghai Synchrotron Radiation Facility (SSRF), utilizing a monochromatic x-ray with a wavelength of 0.6199 Å and a beam size of 2 μm×2 μm. The Raman spectra of the sample at high pressure were recorded by the LabRAM HR Evolution Raman spectrometer from Horiba. Ultraviolet-visible (UV-VIS) and near-infrared (NIR) absorption spectra were collected using optical fiber spectrometers from Ocean Insight, specifically the QE65000 and NIRQuest. The electrical resistance of $AsSbS_3$ under high pressure was measured through the van der Pauw four-probe method, using a Keithley 2400 source meter and a 2182A nanovoltmeter.[23] A composite of cubic boron nitride and epoxy was compressed into a pre-indented metal gasket, creating an insulating layer. A small hole was drilled in the center of this insulating layer using a laser drilling system, and KBr was filled into it to serve as the PTM. Within this layer, four platinum foil electrodes were securely attached.

## 3. Results and discussion

### 3.1. Structural stability of $AsSbS_3$ at high pressure

The *in situ* HP-XRD experiments at room temperature have been conducted to up to 47.0 GPa to investigate the structural behavior of $AsSbS_3$ (Fig. 1(a)). Starting from 4.8 GPa, the HP-XRD pattern of $AsSbS_3$ correspond to the monoclinic structure with the $P2_1/a$ space group (see Fig. S2), representing its stable phase at ambient conditions.[16] As pressure increases, the diffraction peaks of $AsSbS_3$ gradually shift towards higher two theta angle. The intensity of these diffraction peaks decreases and some weaker peaks disappear above 18.6 GPa because of the quasi-hydrostatic pressure and deviatoric stress in the sample chamber. No new diffraction peaks are observed up to 47.0 GPa, indicating the absence of structural phase transitions involving the space group changes.

The unit-cell volume and lattice parameters ($a$, $b$, $c$, and $\beta$ angle) of $AsSbS_3$ gradually decrease with increasing pressure (Fig. 1(c)). The monoclinic $AsSbS_3$ shows a weak anisotropic axial compressibility under high pressure. Upon compression, three axes display similar axial compressibility with the relative more compressible interlayer $c$ axis, followed by the intralayer $a$ and $b$ axes (Fig. S3(a)), which is resulting from the relative weak van der Waals interlayer interactions along $c$ axis. Correspondingly, axial ratios $c/a$, $c/b$, and $b/a$ decrease gradually with increasing pressure, indicating similar axial compressibility and continuous lattice contraction (Fig. S3(b)). Thus, the monoclinic structure of $AsSbS_3$ is stable up to 47.0 GPa without phase transition, and continuous lattice contraction of $AsSbS_3$ upon compression promotes the formation of quasi-three-dimensional framework.

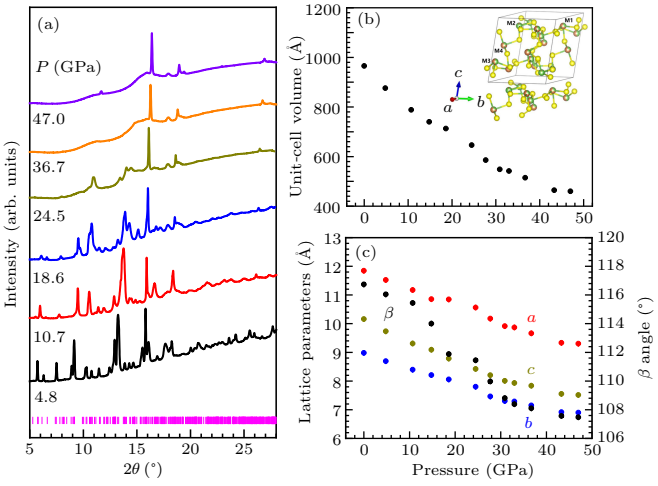



**Fig. 1.** (a) Representative HP-XRD patterns of $AsSbS_3$ under high pressures and room temperature with silicone oil as PTM ($\lambda = 0.6199$ Å). The magenta vertical bars represent the positions of diffraction peaks for $P2_1/a$ phase of $AsSbS_3$. (b) The unit-cell volume of $AsSbS_3$ as a function of pressure. The inset shows the crystal structure of $AsSbS_3$ with the occupancy of As/Sb atoms at the M1–M4 sites. The yellow, brown, and green labeled atoms represent S, Sb, and As, respectively. (c) The lattice parameters of $AsSbS_3$ as a function of pressure, including $a$, $b$, $c$ axes and $\beta$ angle.

The structural behavior of $AsSbS_3$ at high pressure has been compared to other V–VI group $A_2B_3$-type semiconductors, such as stibnite ($Sb_2S_3$) and orpiment ($As_2S_3$). In $Sb_2S_3$, a transition from indirect to direct bandgap and a two-dimensional layered structure to a three-dimensional framework structure are observed before the structural phase transition from *Pnma* to $R\bar{3}m$ at 12.6 GPa.[27,28] As the pressure further increases, several structural phase transitions to $C2/m$, $C2/c$, and $Im\bar{3}m$ are also observed at pressure up to 16.9 GPa, 21.3 GPa, and 47.2 GPa, respectively. Compared to the four phase transitions of $Sb_2S_3$ upon compression, $AsSbS_3$ exhibits structural stability under high pressure, showing similarity to $As_2S_3$, which can be attributed to the higher stability of As–S bonds compared to Sb–S bonds. Although $As_2S_3$ is composed of pyramidal structural units similar to those of $AsSbS_3$, its notably thinner layered structure, compared to $AsSbS_3$, results in a pronounced anisotropic axial compressibility under high pressure. Axial compressibility of interlayer *b* axis in $As_2S_3$ stabilize and the As–S distances converge towards similar values above 25 GPa, indicating an increasing coordination of As atoms and might be related to the completion of three-dimensionalization.[29–31] In contrast, $AsSbS_3$ exhibits gradual lattice contraction throughout the pressure range without any abnormal structural behavior.

The Raman spectrum at room temperature have been performed to investigate the lattice vibrations of $AsSbS_3$ under high pressures (Fig. S5). 16 Raman vibrational peaks are identified in monoclinic $AsSbS_3$ (Fig. S4). The 10 identified Raman characteristic peaks of $AsSbS_3$ that have been reported in previous work can also be found in Fig. S4, which correspond to $P_1$, $P_4$–$P_7$, $P_{10}$–$P_{12}$, $P_{14}$, and $P_{16}$.[19] These vibration modes of $AsSbS_3$ are thought to originate from $A_g$ modes because of its pyramidal structural units ($AsS_3$ and $SbS_3$). As pressure increases, the peak intensity of all modes decreases sharply, becoming almost unrecognizable up to 17.4 GPa. A similar situation is also observed in the control group with Ar used as PTM (Fig. S6). The vibration modes located at 265.99 $cm^{-1}$ and 283.32 $cm^{-1}$ are ascribed to an As/Sb–S stretching mode, shifting to low frequency with negative pressure coefficients.[32] The negative pressure coefficients are associated with vibration softening of crystals, indicating an increasing in As/Sb–S interatomic distances. Additionally, the vibration mode located at 82.46 $cm^{-1}$ is ascribed to another As/Sb–S stretching mode and an $A_1$ mode, showing a well stability under high pressure.[32,33] Moreover, all other modes of vibration exhibit a blue shift as pressure increases, which means the interatomic interaction is significantly enhanced by the compression of the lattice.

As pressure increases, the $AsSbS_3$ crystal undergoes severe amorphization. This is manifested in the experiment as a decrease in the intensity of the diffraction peaks in HP-XRD and the characteristic Raman peaks (Fig. 1(a), Figs. S5 and S6). Although this situation is considered normal under high-pressure conditions related to quasi-hydrostatic pressure and deviatoric stress, such severe amorphization behavior is noticeable. In fact, similar severe amorphization has also been observed in $As_2S_3$.[34] Considering the significant structural differences between them, this behavior is more likely due to natural minerals having more structural defects compared to synthetic materials, rather than an inherent property of these materials. Notably, $As_2S_3$ can withstand much higher pressures (above 36.8 GPa) than $AsSbS_3$, which should be attributed to the greater stability of As–S bonds compared to Sb–S bonds. In addition, the solid solution structure of $AsSbS_3$ may cause it to lose long-range order more easily under high pressure, exacerbating the amorphization phenomenon.

### 3.2. Optical and electrical properties of $AsSbS_3$ at high pressure

To investigate the influence of lattice structural variations under high pressure on the optical and electrical properties of the $AsSbS_3$, optical absorption and electrical transport measurements were conducted up to 24.5 GPa and 37.3 GPa, respectively (Figs. 2 and 3). The sample of $AsSbS_3$ is transparent with a tangerine color at ambient conditions. As pressure increases, the sample shifts towards red, then progressively deepens until it eventually becomes black at 24.5 GPa (Fig. 2(c)). Meanwhile, the absorption edges exhibits a significant red-shift, indicating the narrowing of bandgap (Figs. 2(a) and 2(b)). Furthermore, after releasing pressure to ambient conditions, the absorption edges and crystal color revert to their initial state, suggesting the reversible alteration of the optical bandgap under high pressure (Fig. S7).

Importantly, although $AsSbS_3$ is characterized as a direct bandgap semiconductor, its photoluminescence signal and photocarrier lifetime are associated with the properties of indirect bandgap.[20] Recent research attributes the observed phenomena to the presence of an additional indirect band absorption situated immediately below the direct transition.[35] The energy associated with this indirect band absorption is only marginally inferior to that of the direct transition, potentially resulting in a spectrum that emanates concurrently from both transitional processes. The Tauc plot method relies on the linear extrapolation of the square or square root of the absorption edge energy to determine the bandgap from absorption spectra.[22] In this method, the square and square root correspond to direct and indirect transitions, respectively. Due to the reasons mentioned above, the analysis of spectrum of $AsSbS_3$ should be intermediate between direct and indirect bandgaps. Therefore, we have processed the absorption spectra of the sample according to both types of bandgap

(Fig. 2(d), Figs. S8 and S9). According to Fig. 2(d), the direct bandgap of $AsSbS_3$ is about 2.19 eV at 1.3 GPa, which is slightly larger than the experimental measurement (1.74 eV) but agrees well with the theoretical calculation (2.3 eV).[20,36] As pressure increases, the direct optical bandgap of $AsSbS_3$ gradually decreases to 0.91 eV at 21.5 GPa, maintaining a predominantly linear correlation between the applied pressure and the magnitude of the bandgap. A linear fitting to the direct bandgap upon compression predicts that the bandgap closure occurs around 35 GPa. In comparison, the analysis employing an indirect bandgap fit is also exhibited in Fig. 2(d). An indirect optical bandgap of 2.02 eV is observed at 1.3 GPa, which subsequently decreases to 0.65 eV at the elevated pressure of 21.5 GPa. The indirect bandgap is marginally lower than the direct bandgap counterpart, with an anticipated closure at about 31 GPa. In summary, the optical bandgap of $AsSbS_3$ consistently decreases monotonically as pressure increases. The bandgap exhibits characteristics of reversibility and hysteresis upon decompression, mirroring the behavior observed in absorption edges. It is anticipated that bandgap closure occurs within the pressure range of 31 GPa to 35 GPa, which is affirmed through subsequent electrical transport measurements.

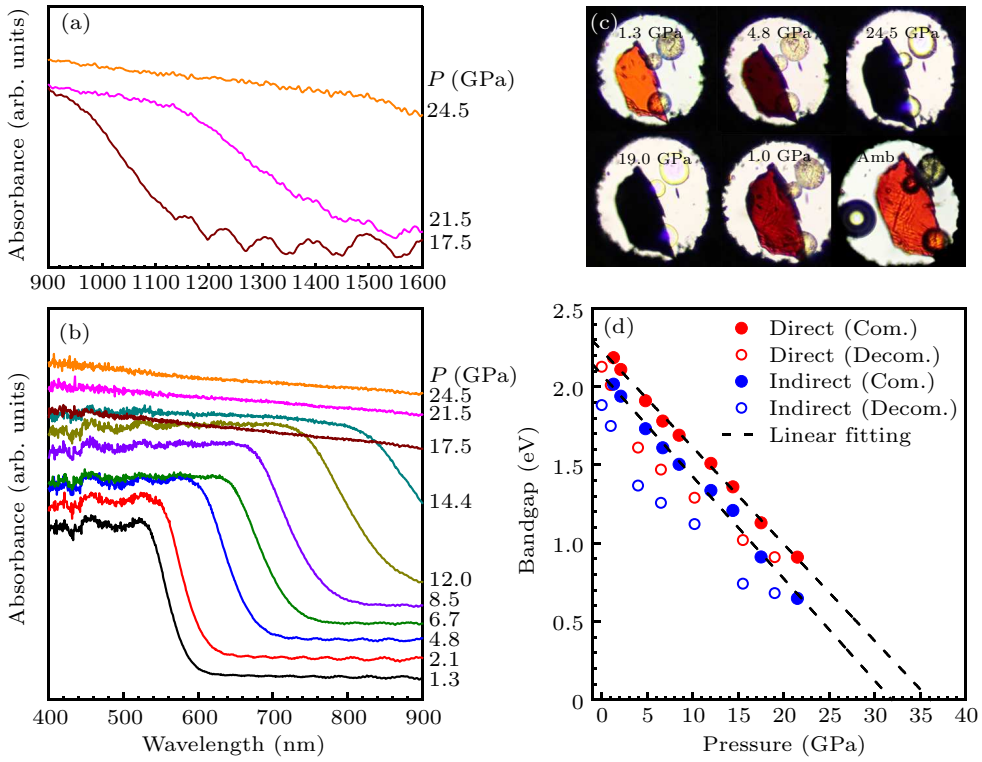



**Fig. 2.** (a) NIR and (b) UV-VIS optical absorption spectra of $AsSbS_3$ at high pressure employing silicone oil as a PTM. (c) Optical images of the sample chamber within a DAC at high pressure. (d) Direct and indirect optical bandgap of $AsSbS_3$ upon compression (Com., solid circles) and decompression (Decom., open circles). The black line denotes the results of linear fitting of compression experimental dataset.

Figure 3(a) shows the temperature-dependent resistance of $AsSbS_3$ in a temperature range of 100 K–280 K at various pressures. At 15.1 GPa, the resistance of $AsSbS_3$ at low temperatures is beyond the measurement capabilities of the instrument, resulting in only data above 170 K being recordable. Nevertheless, the resistance ($R$)–temperature ($T$) curve of $AsSbS_3$ exhibits a negative $dR/dT$ within the measurable temperature range, indicating semiconducting behavior. At higher pressures up to 25.5 GPa, $dR/dT$ is negative at higher temperature range but becomes positive at lower temperature range. Upon further compression to 31.5 GPa, a completely positive $dR/dT$ is observed over the studied temperature range, indicating a metallic state. This semiconductor to metal transition pressure corresponds closely with the bandgap closure pressure range previously predicted in optical absorption experiment. Figure 3(b) shows the pressure-dependent resistivity of $AsSbS_3$ at room temperature. The resistivity of $AsSbS_3$ is calculated by van der Pauw four-electrode method.[23] Under high pressure, the thickness of the sample was determined by considering the compressibility of $AsSbS_3$, which was obtained through HP-XRD experiments under high pressure in this study. Upon compression to around 30 GPa, the resistivity of $AsSbS_3$ drops sharply by approximately four orders of magnitude. When compressed close to and beyond the metallization pressure, the resistivity continues to decrease but at a significantly slower rate. At this point, the change in resistivity with pressure becomes minimal, indicating that most electrons within the crystal can now freely trans-

mit, an important characteristic of the transition from semiconductor to metal. Moreover, this metallization transition under high pressure is reversible upon pressure release.

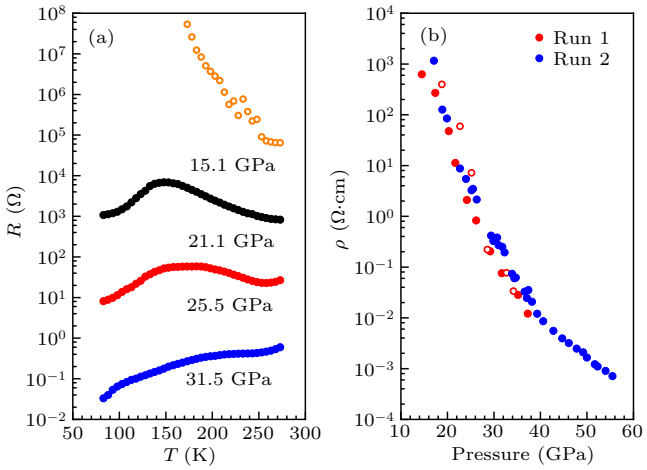



**Fig. 3.** (a) Temperature-dependent resistance of $AsSbS_3$ at high pressures. (b) Resistivity of $AsSbS_3$ was measured by two different runs using the van der Pauw four-electrode method at room temperature. The solid and open circles indicate the experimental data under compression and decompression, respectively.

## 4. Conclusions

In conclusion, the structural behaviors, optical and electrical properties of $AsSbS_3$ at high pressure have been investigated through *in situ* HP-XRD, Raman, optical absorption, and electrical transport measurements. The monoclinic crystal structure of $AsSbS_3$ remains stable up to 47.0 GPa without phase transition. With the lattice contracted continuously, the optical bandgap of $AsSbS_3$ gradually narrows with pressure increasing and is predicted to be close at the range of 31 GPa–35 GPa, indicating gradual metallization of $AsSbS_3$ under compression. The pressure-induced metallization is confirmed by electrical transport experiments. This research could expand the potential applications of $AsSbS_3$ in electronic and optoelectronic industries by high-pressure modulation of crystal structure and physical properties.

## Acknowledgements

Project supported by the National Natural Science Foundation of China (Grant No. 42274123) and the Special Construction Project Fund for Shandong Provincial Taishan Scholars.

## References

[1] Mullen D J E and Nowacki W 1972 *Z. Kristallogr. - Cryst. Mater.* **136** 48
[2] Bayliss P and Nowacki W 1972 *Z. Kristallogr. - Cryst. Mater.* **135** 308
[3] Bolotina N B, Brazhkin V V, Dyuzheva T I, Lityagina L M, Kulikova L F, Nikolaev N A and Verin I A 2013 *Crystallogr. Rep.* **58** 61
[4] Bonazzi P, Menchetti S and Pratesi G 1995 *Am. Miner.* **80** 400
[5] Snyder G J and Toberer E S 2008 *Nat. Mater.* **7** 105
[6] Ghosh C and Varma B P 1979 *Thin Solid Films* **60** 61
[7] Debbichi L, Kim H, Björkman T, Eriksson O and Lebègue S 2016 *Phys. Rev. B* **93** 245307
[8] Vos A D 1980 *J. Phys. D: Appl. Phys.* **13** 839
[9] Pei C, Ying T, Zhang Q, Wu X, Yu T, Zhao Y, Gao L, Li C, Cao W, Zhang Q, Schnyder A P, Gu L, Chen X, Hosono H and Qi Y 2022 *J. Am. Chem. Soc.* **144** 6208
[10] Li Q, Zhang Y J, Xiang Z N, Zhang Y, Zhu X and Wen H H 2024 *Chin. Phys. Lett.* **41** 017401
[11] Zhuang Y and Hu Q 2022 *Chin. Phys. B* **31** 089101
[12] Zheng B, Chen T, Sun H, Yang M, Yang B, Chen X, Zhang Y and Liu X 2024 *Chin. Phys. Lett.* **41** 057301
[13] Shi Y, Wu M, Yue L, Wang K, Li Q, Wu Y, Ye G and Huang H 2024 *Appl. Phys. Lett.* **124** 094103
[14] Luo Y, Shi Y, Wu M, Wu Y, Wang K, Tu B and Huang H 2023 *Appl. Phys. Lett.* **123** 094101
[15] Shi Y, Song H, Li N, Wu X, Wang K, Wu Y, Ye G and Huang H 2022 *Appl. Phys. Lett.* **121** 114101
[16] Weissberg B G 1965 *Am. Min.* **50** 1817
[17] Guillermo T R and Wuensch B J 1973 *Acta Crystallogr. Sect. B-Struct. Sci.Cryst. Eng. Mat.* **29** 2536
[18] Kyono A and Kimata M 2004 *Am. Miner.* **89** 696
[19] Tripathi R P N, Yang X and Gao J 2021 *Laser Photon. Rev.* **15** 2100182
[20] Wang P, He D, He J, Fu J, Liu S, Han X, Wang Y and Zhao H 2020 *J. Phys. Chem. A* **124** 1047
[21] Kumar N, He J, He D, Wang Y and Zhao H 2013 *J. Appl. Phys.* **113** 133702
[22] Tauc J 1968 *Mater. Res. Bull.* **3** 37
[23] Pauw L J V D 1991 *Semiconductor Devices: Pioneering Papers* pp. 174–182
[24] Kantor I, Prakapenka V, Kantor A, Dera P, Kurnosov A, Sinogeikin S, Dubrovinskaia N and Dubrovinsky L 2012 *Rev. Sci. Instrum.* **83** 125102
[25] Akahama Y and Kawamura H 2004 *J. Appl. Phys.* **96** 3748
[26] Mao H K, Bell P M, Shaner J W and Steinberg D J 1978 *J. Appl. Phys.* **49** 3276
[27] Wang Y, Ma Y, Liu G, Wang J, Li Y, Li Q, Zhang J, Ma Y and Zou G 2018 *Sci. Rep.* **8** 14795
[28] Cui Z, Bu K, Zhuang Y, Donnelly M-E, Zhang D, Dalladay-Simpson P, Howie R T, Zhang J, Lü X and Hu Q 2021 *Commun. Chem.* **4** 125
[29] Cuenca-Gotor V P, Sans J A, Gomis O, Mujica A, Radescu S, Munoz A, Rodriguez-Hernandez P, da Silva E L, Popescu C, Ibanez J, Vilaplana R and Manjon F J 2020 *Phys. Chem. Chem. Phys.* **22** 3352
[30] Liu K, Dai L, Li H, Hu H, Yang L, Pu C, Hong M and Liu P 2019 *Materials* **12** 784
[31] Struzhkin V V, Goncharov A F, Caracas R, Mao H K and Hemley R J 2008 *Phys. Rev. B* **77** 165133
[32] Parize R, Cossuet T, Chaix-Pluchery O, Roussel H, Appert E and Consonni V 2017 *Mater. Des.* **121** 1
[33] Razzetti C and Lottici P P 1979 *Solid State Commun.* **29** 361
[34] Qin T, Shi Y, Wu M, Tu B, Wu Y, Wang K and Huang H 2024 *Phys. Scr.* **99** 095940
[35] Sabik A, Grodzicki M, Polak M P, Gorantla S, Bachmatiuk A, Kudrawiec R and Linhart W M 2024 *APL Mater.* **12** 031122
[36] Lazaar K, Gueddida S, Pascale F, Said M and Lebègue S 2022 *Phys. Status Solidi B-Basic Solid State Phys.* **260** 2200592